

New Evidence for Mass-Loss from δ Cephei from H I 21-cm Line Observations

L. D. Matthews¹, M. Marengo², N. R. Evans³, & G. Bono^{4,5}

ABSTRACT

Recently published *Spitzer Space Telescope* observations of the classical Cepheid archetype δ Cephei revealed an extended dusty nebula surrounding this star and its hot companion HD 213307. At far infrared wavelengths, the emission resembles a bow shock aligned with the direction of space motion of the star, indicating that δ Cephei is undergoing mass-loss through a stellar wind. Here we report H I 21-cm line observations with the Very Large Array (VLA) to search for neutral atomic hydrogen associated with this wind. Our VLA data reveal a spatially extended H I nebula ($\sim 13'$ or 1 pc across) surrounding the position of δ Cephei. The nebula has a head-tail morphology, consistent with circumstellar ejecta shaped by the interaction between a stellar wind and the interstellar medium (ISM). We directly measure a mass of circumstellar atomic hydrogen $M_{\text{HI}} \approx 0.07 M_{\odot}$, although the total H I mass may be larger, depending on the fraction of circumstellar material that is hidden by Galactic contamination within our band or that is present on angular scales too large to be detected by the VLA. It appears that the bulk of the circumstellar gas has originated directly from the star, although it may be augmented by material swept from the surrounding ISM. The H I data are consistent with a stellar wind with an outflow velocity $V_{\infty} = 35.6 \pm 1.2 \text{ km s}^{-1}$ and a mass-loss rate of $\dot{M} \approx (1.0 \pm 0.8) \times 10^{-6} M_{\odot} \text{ yr}^{-1}$. We have computed theoretical evolutionary tracks that include mass loss across the instability strip and show that a mass-loss rate of this magnitude, sustained over the preceding Cepheid lifetime of δ Cephei, could be sufficient to resolve a significant fraction of the discrepancy between the pulsation and evolutionary masses for this star.

¹Massachusetts Institute of Technology Haystack Observatory, Off Route 40, Westford, MA 01886 USA

²Department of Physics & Astronomy, Iowa State University, Ames, IA 50011 USA

³Harvard-Smithsonian Center for Astrophysics, 60 Garden Street, MS-42, Cambridge, MA 02138 USA

⁴Department of Physics, Università di Roma Tor Vergata via Della Ricerca Scientifica 1, 00133 Roma, Italy

⁵INAF, Rome Astronomical Observatory, via Frascati 33, 00040 Monte Porzio Catone, Italy

Subject headings: (stars: variables:) Cepheids – stars: mass loss – stars: Individual (δ Cephei) – radio lines: stars – (stars:) circumstellar matter

1. Introduction

Owing to the tight coupling between the pulsation properties of Cepheid variables and their fundamental stellar parameters, these stars have long provided crucial tests for stellar evolution models (Gautschi & Saio 1996) and play a key role in the calibration of the extragalactic distance scale (Feast & Walker 1987; Freedman et al. 2001). Nonetheless, for more than 40 years, a puzzle has persisted concerning the lingering discrepancy between stellar masses derived for Cepheids using different methods (e.g., Cox 1980). In spite of improved radiative opacity calculations (Iglesias et al. 1990; Seaton et al. 1994), advances in evolutionary modeling (Bono et al. 2002), and the consideration of metallicity effects (Keller & Wood 2006), masses derived from stellar evolutionary models are found to be systematically $\sim 10\text{--}15\%$ higher than those derived from stellar pulsation models (Caputo et al. 2005) or orbital dynamics, when available (Evans 2009).

As described by Neilson et al. (2011), one of the most promising solutions to the so-called “Cepheid mass discrepancy” is likely to be convective core overshooting (Chiosi et al. 1992) coupled with *mass-loss* during the Cepheid phase of evolution (see also Bono et al. 2006). Mass-loss from Cepheids has long been postulated, not only as a means of resolving the Cepheid mass discrepancy, but as a natural consequence of stellar evolution and pulsation models (e.g., Iben 1974; Willson & Bowen 1984; Neilson & Lester 2008). The observational confirmation of mass loss from Cepheids would impact not only our understanding of Cepheid evolution, but would also have implications for the use of Cepheids as distance indicators. For example, mass-loss can non-negligibly affect the structure and scatter in the infrared period-luminosity relation (Neilson et al. 2009), and the presence of circumstellar material can impact Cepheid distance determinations made using the interferometric Baade-Wesselink method (Mérand et al. 2007).

A number of previous authors have attempted to identify direct evidence of past or ongoing mass-loss from Cepheids using observations ranging from ultraviolet to radio wavelengths (e.g., Deasy & Butler 1986; Deasy 1988; Welch & Duric 1988; Bohm-Vitense & Love 1994; Mérand et al. 2007; Kervella et al. 2006, 2009; Neilson et al. 2009). However, the results have been inconclusive, as the mass-loss rates (or upper limits) derived from these studies ($\dot{M} \approx 10^{-12}$ to $10^{-5} M_{\odot} \text{ yr}^{-1}$) span many orders of magnitude and are typically rather uncertain owing to their reliance on trace atomic and molecular species (which may not be optimal tracers of past and ongoing mass-loss), their inability to sample very extended

spatial scales, and finally, the strong dependencies of derived mass-loss rates on a variety of underlying assumptions (e.g., wind structure, gas-to-dust ratios, ionization fractions).

With the goal of obtaining new empirical constraints on Cepheid mass-loss, Marengo et al. (2010a) recently used the *Spitzer Space Telescope* to survey a sample of 29 nearby Cepheids. While IR excesses were not directly detected, ruling out the presence of a large amount of warm (~ 500 K) dust in close proximity to the stars, the *Spitzer* images revealed extended emission around several targets (Marengo et al. 2010a; Barmby et al. 2011). Perhaps the most intriguing was the discovery of a prominent nebula around the archetype Cepheid variable, δ Cephei (Marengo et al. 2010b).

Some basic stellar properties of δ Cephei are summarized in Table 1. δ Cephei is part of a wide binary (Benedict et al. 2002), with a hot companion HD 213307 ($T_{\text{eff}} = 8800$ K; Cenarro et al. 2007) separated by a projected distance of $40''$. The IR emission surrounding δ Cephei (and HD 213307) is visible in multiple *Spitzer* bands and shows a roughly parabolic structure with an extent of $\sim 5'$ ($\approx 2 \times 10^4$ AU). The symmetry axis of the parabola is aligned with the direction of the star’s motion through the interstellar medium (ISM; Marengo et al. 2010b), where $V_{\text{space}} \approx 10.3 \text{ km s}^{-1}$ and P.A. = $58^\circ.3$.¹ The IR emission therefore appears to trace a bow shock structure, as arises when a moving, mass-losing star interacts with the local ISM (e.g., Wilkin 1996). Bow shocks have been seen previously in FIR images of a number of mass-losing stars, including the supergiants α Cam (Van Buren & McCray 1988) and α Ori (Noriega-Crespo et al. 1997; Ueta et al. 2008) and the asymptotic giant branch (AGB) stars R Hya (Ueta et al. 2006; Wareing et al. 2006), Mira (Ueta 2008), R Cas (Ueta et al. 2010), IRC+10216 (Ladjal et al. 2010), TX Psc, and X Her (Jorissen et al. 2011). The emission mechanism responsible for the FIR emission from these circumstellar bow shocks is uncertain, but is likely to be mainly thermal emission from dust, with possible contributions from low-excitation atomic emission lines (Ueta et al. 2008; Marengo et al. 2010b).

While the companion of δ Cephei, HD 213307, cannot strictly be excluded as the source of the IR emitting material seen by *Spitzer*, this appears quite unlikely based on the B7-B8 III-V spectral type of this star (see Marengo et al. 2010b for discussion). Thus the *Spitzer* observations of Marengo et al. (2010b) provide strong evidence that δ Cephei is undergoing mass loss through a stellar wind. To further characterize the nature of this wind and its interaction with the ISM, we have now used the Very Large Array (VLA) to search for H I 21-cm line emission in the circumstellar environment of δ Cephei.

H I observations have been used previously to trace extended circumstellar emission sur-

¹For the present work, we have recomputed the space motion vector for δ Cephei using the updated solar constants from Schönrich et al. 2010.

rounding a number of mass-losing AGB stars (e.g., Gérard & Le Bertre 2006; Matthews & Reid 2007; Libert et al. 2008; Matthews et al. 2008, 2011). Frequently, the H I emission associated with AGB stars is highly extended (up to ~ 1 pc) and shows signatures of interaction with the ISM in the form of trailing H I wakes, velocity gradients caused by ram pressure effects, and/or density enhancements that demarcate the interstellar-circumstellar interaction zone. Furthermore, several of the evolved stars detected in H I are among those with FIR (and/or FUV) emitting bow shocks, including Mira, R Cas, and IRC+10216, underscoring the complementarity of these tracers for probing the chemistry and kinematics of stellar outflows and their interaction with their environments. This paper represents the first extension of this approach to the study of Cepheids.

2. VLA Observations

H I 21-cm line observations of δ Cephei were obtained using the VLA of the National Radio Astronomy Observatory (NRAO)² during four observing sessions in 2009 (see Table 2). All data were obtained using the compact (D) configuration (0.035-1.0 km baselines), providing sensitivity to emission on scales of up to $\sim 15'$. The primary beam of the VLA at the observing frequency of 1420.5 MHz is $\sim 31'$.

The VLA correlator was used in 1A mode with a 1.56 MHz bandpass, yielding 512 spectral channels with 3.05 kHz (~ 0.64 km s⁻¹) spacing in a single (right circular) polarization. The band was centered at a velocity of -7.5 km s⁻¹ relative to the local standard of rest (LSR). In total, ~ 15.1 hours of integration were obtained on δ Cephei. Approximately 20% of the observed visibilities were flagged because of radio frequency interference (RFI) or hardware problems. Observations of δ Cephei were interspersed with observations of a phase calibrator, 2203+626, approximately every 20 minutes. 3C48 (0137+331) was used as a flux calibrator, and an additional strong point source (2253+161) was observed as a bandpass calibrator (Table 2). To insure that the absolute flux scale and bandpass calibration were not corrupted by Galactic emission in the band, the flux and bandpass calibrators were each observed twice, with frequency shifts of +1.1 MHz and -1.7 MHz, respectively, relative to the band center used for the observations of δ Cephei and 2203+626. 2203+626 was also observed once at each of these offset frequencies to permit more accurate bootstrapping of the absolute flux scale to the δ Cephei data, although in some cases, one of the offset scans had to be discarded (see Table 2). We estimate that the resulting absolute flux scale has an

²The National Radio Astronomy Observatory is operated by Associated Universities, Inc., under cooperative agreement with the National Science Foundation.

Table 1. Coordinates and Stellar Properties of δ Cephei

Parameter	Value	Ref.
α (J2000.0)	22 29 10.2	1
δ (J2000.0)	+58 24 54.7	1
l	105°19	1
b	+0°53	1
Distance (pc)	273±0.011	2
Spectral Type	F5Ib-G1Ib	3
Pulsation period (days)	5.366341	3
Mean T_{eff} (K)	5910	4
Mass (pulsation) ^b (M_{\odot})	4.5±0.3	5
Mass (evolutionary) ^c (M_{\odot})	5.7±0.5	5
Mean M_V	−3.47±0.10	2
Mean Luminosity (L_{\odot})	~2000	...
Mean radius (R_{\odot})	44.5 ^a	6
V_{LSR}^d	−4.7 km s ^{−1}	7

^aBased on the mean, limb darkened angular diameter $\phi_{\text{LD}}=1.520$ mas and the distance adopted here.

^bBased on $V - K$ colors.

^cAssuming a canonical model with no overshoot; see § 4.5).

^dDerived from the heliocentric radial velocity $V_h = -16.8$ km s^{−1}.

Note. — Units of right ascension are hours, minutes, and seconds, and units of declination are degrees, arcminutes, and arcseconds. All quantities have been scaled to the distance adopted in this paper.

References. — (1) SIMBAD database; (2) Benedict et al. 2002; (3) Samus et al. 2011; (4) Andrievsky et al. 2005; (5) Caputo et al. 2005; (6) Armstrong et al. 2001; (7) Wilson 1953

uncertainty of $\sim 10\%$.

The data were calibrated and imaged using the Astronomical Image Processing System (AIPS). At the time of our observations, the VLA contained 22 operational antennas with L-band receivers, 20 of which had been retrofitted as part of the Expanded Very Large Array (EVLA) upgrade. Data obtained during this EVLA transition period require special care during calibration.³ After applying the latest available corrections to the antenna positions and performing an initial excision of corrupted data, we computed and applied a bandpass calibration to our spectral line data to remove closure errors on VLA-EVLA baselines. The bandpass was normalized using channels 163–448, thus excluding the portion of the band affected by aliasing. We next computed a frequency-averaged (channel 0) data set for use in calibrating the frequency-independent complex gains, again using channels 163–448. Following gain calibration, we applied time-dependent frequency shifts to the data to compensate for changes caused by the Earth’s motion during the course of the observations. At this stage, we also applied hanning smoothing in velocity and discarded every other channel, yielding a 256 channel data set with a velocity resolution of $\sim 1.3 \text{ km s}^{-1}$.

Prior to imaging the line data, the u - v data were continuum-subtracted using a zeroth order fit to the real and imaginary components of the visibilities. Channels 20–95 of the hanning-smoothed data set (corresponding to an LSR velocity range of 35.6 to 132.2 km s^{-1}) were determined to be line-free and were used for these fits. Although the spectral shape of the aliased portion of the continuum was better approximated by a higher order polynomial, the weakness of the continuum in the line data coupled with the lack of line-free channels on the high-frequency end of the band did not provide adequate constraints for a higher order fit.

We imaged the H I line data using the standard AIPS CLEAN deconvolution algorithm and produced data cubes using various weighting schemes. Some characteristics of these cubes are summarized in Table 3. Additionally, we produced an image of the 21-cm continuum emission in the δ Cephei field using the line-free portion of the band. The peak continuum flux density within the primary beam was $\sim 0.5 \text{ Jy}$ (after correction for beam attenuation). We compared the measured flux densities of several sources in the field with those from the NRAO VLA Sky Survey (Condon et al. 1998) and found agreement to within $\lesssim 7\%$. We did not detect any continuum emission at or near the position of δ Cephei and place a 3σ upper limit on the 21-cm continuum flux density at the stellar position of $F_{\text{cont}} < 1.0 \text{ mJy}$. This is consistent with the results of Welch & Duric (1988), who found no evidence of significant mass-loss from δ Cephei in the form of an ionized wind based on radio

³See <http://www.vla.nrao.edu/astro/guides/evlaretturn/>.

continuum observations at 5 GHz.

3. Results

Figure 1 shows a series of H I channel maps extracted from our Tapered VLA data cube (see Table 3). Only a few representative channels are shown blueward of the stellar systemic velocity ($V_{\text{LSR}} = -4.7 \text{ km s}^{-1}$), as this portion of our band was strongly contaminated by large-scale Galactic emission along the line-of-sight. This emission is poorly spatially sampled by the VLA, resulting in patterns of positive and negative mottling across the channel images. To better illustrate the character of the Galactic emission, Figure 2 presents a single-dish H I survey spectrum from Kalberla et al. (2005), which shows H I emission with a brightness temperature as high as $\sim 85 \text{ K}$ toward the direction of δ Cephei. Both the strength and spatial complexity of this emission hampered our search for circumstellar signals over the velocity range $-125 \lesssim V_{\text{LSR}} \lesssim 12.5 \text{ km s}^{-1}$.

Fortunately, the spectrum in Figure 2 reveals that the Galactic H I emission drops precipitously for $V_{\text{LSR}} \gtrsim 13 \text{ km s}^{-1}$, providing a clean band over which to search for circumstellar emission. Because the outflow velocities from Cepheids are expected to be at least a few tens of km s^{-1} (e.g., Deutsch 1960; Reimers 1977; Holzer & MacGregor 1985), this velocity window is of prime interest for searching for circumstellar emission associated with δ Cephei.

Consistent with the total power spectrum in Figure 2, we see in Figure 1 that the pattern in the VLA images caused by large-scale Galactic emission diminishes near $V_{\text{LSR}} = 13.8 \text{ km s}^{-1}$. Furthermore, that same channel exhibits an extended H I emission region centered near the position of δ Cephei. Looking toward higher velocities, we find a series of 15 contiguous channels where spatially extended H I emission is detected coincident with the position of δ Cephei. Several marginally extended features of $\sim 3\sigma$ significance are also seen clustering near the stellar position in each of the next five contiguous channels, out to $V_{\text{LSR}} = 38.2 \text{ km s}^{-1}$.

In Figure 3 we present velocity-integrated H I total intensity contours, derived from data spanning the velocity range $13.8 \leq V_{\text{LSR}} \leq 38.2 \text{ km s}^{-1}$. These contours are overlaid on the *Spitzer* $24\mu\text{m}$ and $70\mu\text{m}$ maps, respectively, from Marengo et al. (2010b). Some caution is required in interpreting the detailed morphology of the velocity-integrated H I distribution in Figure 3, as additional material associated with this nebula is likely to be present at lower velocities, where it cannot be disentangled from the prominent Galactic emission. However, despite this caveat, several characteristics of the integrated H I emission seen in Figure 3 are strongly indicative of an association with the circumstellar environment of δ Cephei.

Table 2. VLA Calibration Sources

Source	α (J2000.0)	δ (J2000.0)	Flux Density (Jy)	Date
3C48 ^a	01 37 41.29	+33 09 35.13	15.88*	All
2253+161 ^b	22 53 57.74	+16 08 53.56	13.74 \pm 0.15 [†]	2009-Oct-28
...	13.46 \pm 0.28**	2009-Nov-15&16
...	13.27 \pm 0.23**	2009-Nov-22&23
...	13.36 \pm 0.22 [†]	2009-Nov-27&28
2203+626 ^c	22 03 20.96	+62 40 34.27	2.75 \pm 0.02**	2009-Oct-28
...	2.72 \pm 0.01**	2009-Nov-15&16
...	2.73 \pm 0.01**	2009-Nov-22&23
...	2.75 \pm 0.01 ^{††}	2009-Nov-27&28

Note. — Units of right ascension are hours, minutes, and seconds, and units of declination are degrees, arcminutes, and arcseconds.

*Adopted flux density at 1420.5 MHz, computed according to the VLA Calibration Manual (Perley & Taylor 2003).

[†]Computed flux density at 1419.2 MHz; data at 1422.1 MHz were corrupted.

**Mean computed flux density from observations at 1419.2 and 1422.1 MHz; see § 2.

^{††}Computed flux density at 1422.1 MHz; data at 1419.2 MHz were corrupted.

^aPrimary flux calibrator

^bBandpass calibrator

^cPhase calibrator

Table 3. Deconvolved Image Characteristics

Image Descriptor (1)	\mathcal{R} (2)	Taper (k λ ,k λ) (3)	θ_{FWHM} (arcsec) (4)	PA (degrees) (5)	rms (mJy beam ⁻¹) (6)
Robust +1	+1	...	49'' \times 45''	20°3	1.6
Natural	+5	...	54'' \times 49''	21°7	1.5
Tapered	+5	2,2	97'' \times 89''	2°5	1.8
Continuum	-1	...	39'' \times 36''	0°3	0.39

Note. — Explanation of columns: (1) image or data cube designation used in the text; (2) AIPS robustness parameter used in image deconvolution; (3) Gaussian taper applied in the u and v directions, expressed as distance to 30% point of Gaussian in units of kilolambda; (4) dimensions of synthesized beam; (5) position angle of synthesized beam (measured east from north); (6) mean rms noise per channel (1σ) in the unaliased portion of the band (line data) or in frequency-averaged data (continuum).

One of the most intriguing aspects of the H I emission distribution in Figure 3 is its “head-tail” morphology. This is reminiscent of the structures of the extended circumstellar envelopes of several of the AGB stars that have been imaged in H I, FIR and/or FUV light (Martin et al. 2007; Matthews et al. 2008, 2011; Ueta 2008; Sahai & Chronopoulos 2010; Jorissen et al. 2011) and results when material shed by a stellar wind is swept by ram pressure into a trailing wake as the star transverses the ISM (e.g., Wareing et al. 2007b). The direction of space motion of δ Cephei, indicated by an arrow on Figure 3, strongly supports an analogous interpretation for the H I nebula surrounding this star. We see that the maximum angular extent of the H I nebula ($\sim 13'$, corresponding to ~ 1.0 pc at the distance of δ Cephei) is aligned with the space motion direction. Furthermore, the distribution of the H I nearest to the position of δ Cephei ($r \lesssim 2'$) is well correlated with the distributions of both the $24\mu\text{m}$ and $70\mu\text{m}$ emissions detected by *Spitzer*. The H I emission thus appears to be associated with the same dusty wind traced by the IR data.

The peak of the H I column density in Figure 3 ($N_{\text{HI}} \approx 2.0 \times 10^{19} \text{ cm}^{-2}$) does not correspond to the position of δ Cephei or its companion HD 213307 (indicated on Figure 3 by a star and cross symbol, respectively), but rather lies $\sim 112''$ to the northeast of δ Cephei, near the apex of the shock structure delineated by the IR emission. Such an offset of the peak emission from the star is not surprising, as this kind of leading density enhancement is a hallmark of the “snowplow” effect that may occur when a wind-emitting star moves supersonically through the ambient medium (Isaacman 1979; Raga et al. 2008).

To the west of δ Cephei, i.e., downstream from the star’s trajectory, our VLA image reveals a wake of material trailing the motion of the star. In contrast to the gaseous wakes associated with stars such as Mira (Matthews et al. 2008) and X Her (Matthews et al. 2011), the material downstream from δ Cephei is not well collimated and more closely resembles the wide-angle “vortical tail” associated with the carbon star IRC+10216 (Sahai & Chronopoulos 2010). Numerical simulations of the interactions between stellar winds and streaming environments frequently predict broad, turbulent wakes, qualitatively similar to what we see in Figure 3 (e.g., Wareing et al. 2007a), although the degree of collimation and other properties of circumstellar wakes are highly sensitive to the stellar velocity, properties of the stellar wind, and the density of the ambient medium (Comerón & Kaper 1998), such that fully unraveling the interplay between these factors for a particular source generally requires a specifically tailored model.

To gauge the total mass of H I giving rise to the emission seen in Figures 1 and 3 over the velocity range $V_{\text{LSR}}=15.0$ to 38.2 km s^{-1} , we have summed the emission surrounding the stellar position (after correction for primary beam attenuation) in irregularly shaped blotches defined by 3σ brightness contours. This approach yielded an integrated H I flux

density of $\int S_v dv = 4.1 \pm 0.2 \text{ Jy km s}^{-1}$. Using the relation $M_{\text{HI}} = 2.36 \times 10^{-7} d^2 \int S_v dv M_{\odot}$ where d is the stellar distance in pc (e.g., Roberts 1975), this translates to an HI mass of $M_{\text{HI}} \approx 0.07 M_{\odot}$. While this approach for measuring the total HI context minimizes the contribution of background noise to the measurement, it may result in the exclusion of weak emission or emission from regions not contiguous with the primary emission region in each channel. For comparison, we therefore summed the emission in each channel over a fixed rectangular aperture ($16'.6 \times 13'.3$, centered $100''$ west of δ Cephei's position). We found $S_v = 4.4 \pm 0.4 \text{ Jy km s}^{-1}$, consistent with our first estimate.

We interpret our measured integrated HI flux density as a lower limit to the amount of circumstellar material present around δ Cephei for two reasons. First, additional emission may lie undetected at velocities where our spectral images were contaminated by Galactic emission. For example, if we assume that the HI line profile is symmetric about the systemic velocity of δ Cephei, this would imply that roughly two-thirds of the channels containing circumstellar signal were excluded from our flux density measurement. Secondly, at our observing frequency, the VLA D configuration is only sensitive to emission on angular scales $\lesssim 15'$. Since this is comparable to the angular extent of the observed HI nebula surrounding δ Cephei, it is plausible that we have missed additional extended emission. This problem could be exacerbated if the most spatially extended material is decelerated as a result of its interaction with the ISM (e.g., Matthews et al. 2008); this could in turn cause its velocity to be blueshifted into the portion of our band contaminated by Galactic emission. Mapping the region in HI with a single-dish telescope would be of considerable interest as a means of searching for an additional large-scale emission component.

4. Discussion

4.1. How Robust is the Association between the HI Nebula and δ Cephei?

The Galactic ISM is well known to exhibit structures on wide variety of scales, down to arcminutes and below (e.g., Verschuur 1974; Greisen & Liszt 1986; Heiles & Troland 2003; Begum et al. 2010). We therefore have considered the possibility that the HI nebula that we have detected toward δ Cephei could simply be a chance superposition of an unrelated HI cloud along the line-of-sight. However, several lines of evidence indicate that this is extremely unlikely.

As described above, the close correspondence between the HI emission contours surrounding δ Cephei and the bow shock structure traced by FIR emission implies that the two are linked. Since the formation of a bow shock requires a stellar wind, a linkage between the

H I and FIR emission argues strongly against the former arising from a random interstellar cloud.

Based on a survey with the Arecibo L -band Feed Array, Begum et al. (2010) identified a population of compact H I clouds associated with the Galactic plane (but distinct from the main Galactic disk emission) whose column densities and angular sizes overlap with those characterizing the H I nebula that we have detected toward δ Cephei. However, the mean characteristic linewidth of the clouds catalogued by Begum et al. is $\Delta V = 4.2 \text{ km s}^{-1}$ (FWHM), with values generally lying in the range of $\sim 1\text{--}8 \text{ km s}^{-1}$. Only a handful of the 96 clouds in their sample exhibit velocity widths comparable to or larger than that of the integrated linewidth of the δ Cephei nebula ($\Delta V \approx 12.6 \text{ km s}^{-1}$ based on a Gaussian fit). Furthermore, while Begum et al. have underscored the possibility that a subset of their compact clouds may in fact be associated with mass-loss from variable stars, the closest association that they identified between a catalogued variable and a cloud from their sample has a projected separation of $10'$. Since the H I properties of the δ Cephei nebula are somewhat atypical of the general population of compact Galactic clouds, we conclude that the probability of detecting such a cloud with a head-tail morphology at both the position and velocity expected for δ Cephei, is extraordinarily small.

4.2. The Stellar Mass-Loss Rate

4.2.1. New Estimates of \dot{M} Based on the VLA Data

One of the most powerful applications of our VLA measurements is that they allow us to obtain new, independent constraints on the mass-loss rate from δ Cephei. Two key advantages of H I observations for characterizing stellar mass-loss are first, that the H I mass can be derived directly from the observed emission (assuming it is optically thin) and secondly, that spectroscopic imaging of H I is sensitive to material much farther from the star than most other observational techniques for probing stellar mass loss, thereby tracing a larger fraction of the total mass-loss history.

We consider two independent approaches for estimating the mass loss rate of δ Cephei from our VLA data. Our first method is to adopt a simplified model in which the star is assumed to be undergoing mass-loss through an isothermal, spherically symmetric wind that is in free expansion out to some radius $r = R_0$. While pulsation-driven winds are inherently non-steady, we assume that the outflow can be approximated as quasi-steady when averaged over the timescales sampled by our observations.

In the case where the H I emission is optically thin, a theoretical line profile as a function

of velocity, V , for this idealized wind can be written as:

$$S(V) = \frac{2f\sqrt{\pi\ln 2} \dot{M}}{4d\pi BV_o^2(1.83 \times 10^{18})\mu m_H \left[1 - \left(\frac{V}{V_o}\right)^2\right]^{0.5}} \text{erf}(x_{\max}) \text{ mJy} \quad (1)$$

where

$$x_{\max} = \frac{2\sqrt{\ln 2}R_0}{B} \left[1 - \left(\frac{V}{V_o}\right)^2\right]^{0.5}$$

(see Knapp & Bowers 1983; Olofsson et al. 1993). Here f is the conversion factor between units of brightness temperature in kelvins and mJy per beam for the radio telescope used, d is the distance to the star, B is the half-power synthesized beamwidth of the telescope, V_o is the outflow velocity of the wind, μ is the mean atomic weight of the gas (taken to be 1.3), and m_H is the mass of the hydrogen atom. All quantities are expressed in cgs units.

For comparison with the theoretical profile, we extracted from the VLA data a spectrum, averaged over a single synthesized beam centered on δ Cephei. We used the “Robust+1” data cube for this analysis (Table 3), which has the highest angular resolution and should minimize contamination from structures in the H I envelope that are expected to lie outside the freely expanding wind (e.g., material in the tail and/or bow shock). We then compared the observed spectrum with a series of models where the mass-loss rate and wind outflow speed were taken as free parameters. Before comparison with the data, each model computed from Eq. 1 was convolved with a broadening kernel to account for the finite spectral resolution and the gas turbulence. The model parameters were constrained by scanning a grid of possible values and minimizing χ^2 . The outflow velocity, mass-loss rate, and smoothing kernel were incremented by values of 0.1 km s^{-1} , $1 \times 10^{-8} M_\odot \text{ yr}^{-1}$, and 0.1 km s^{-1} , respectively. The best-fitting model profile is overplotted on the observed spectrum in Figure 4. The model parameters are $V_o = 35.6 \pm 1.2 \text{ km s}^{-1}$, $\dot{M} = (1.7 \pm 0.1) \times 10^{-6} M_\odot \text{ yr}^{-1}$, and $\sigma_{\text{turb}} = 1.8 \pm 0.2 \text{ km s}^{-1}$. The quoted uncertainties do not reflect the uncertainties in parameters held fixed in the model, namely the stellar systemic velocity, the envelope radius, and the distance to the star. Our model underestimates the peak H I flux density of the observed spectrum, which may reflect uncertainties in the fixed parameters of the model (e.g., the envelope radius) or be due to contamination of the observed spectrum by swept-up interstellar gas and/or gas from outside the free expansion zone of the wind. It may also reflect a breakdown of our highly idealized model (e.g., owing to highly episodic mass-loss or a latitude dependent wind).

A second, independent means of constraining the mass-loss rate from the H I data comes

from the total mass of circumstellar H I emission observed, coupled with available constraints on the timescale for the mass-loss. Over the velocity range $13.8 \leq V_{\text{LSR}} \leq 38.2 \text{ km s}^{-1}$, we directly measured a total H I mass of $0.07 M_{\odot}$ from material that appears to be associated with the circumstellar environment of δ Cephei (see § 3). Applying a multiplicative correction of 1.34 to account for the mass of helium yields $M_{\text{tot}} \gtrsim 0.09 M_{\odot}$. As noted above, we regard this as a lower limit to the total envelope mass, since additional circumstellar emission may lie in portions of our band that are contaminated by Galactic signal and/or at large angular scales to which the VLA is insensitive.

The tail of H I emission downstream from δ Cephei has an extent of $\sim 500''$, or $2 \times 10^{18} \text{ cm}$ in the plane of the sky. Assuming a tangential velocity of 7 km s^{-1} (derived from the observed stellar radial velocity and proper motions as described in Marengo et al. 2010b and the new solar constants of Schönrich et al. 2010), the crossing time for the nebula is $\sim 90,600 \text{ yr}$. For the total circumstellar mass above, this would imply a mean mass-loss rate of $\dot{M} \approx 1 \times 10^{-6} M_{\odot} \text{ yr}^{-1}$. While this is comparable to the rate derived from our model fitting above, the actual mass-loss rate could be smaller if some fraction of the observed H I gas arises from swept-up interstellar material rather than directly from stellar mass-loss (see § 4.2.2 below). Moreover, the dynamical crossing time of a stellar wake provides only a lower limit to its age (see Matthews et al. 2008); if δ Cephei has been losing mass over a more prolonged interval, \dot{M} would also be lower. We note, however, that δ Cephei is believed to be on its second crossing of the Cepheid instability strip (Berdnikov et al. 2000; Turner et al. 2006), and the total duration of this phase for a star of its mass and metallicity is expected to be $\sim (1.3\text{--}5.9) \times 10^5 \text{ yr}$ (see § 4.5). These numbers are only a few times larger than our estimated dynamical age, suggesting that the mean mass loss rate cannot be significantly lower than we have inferred under the assumption that all of the observed mass-loss occurred during the Cepheid phase. [The duration of the first Cepheid crossing ($\sim 15,000 - 30,000 \text{ yr}$ for a star like δ Cephei; see § 4.5) is too short to impact this conclusion]. On the other hand, if we have underestimated the amount of emission in the H I nebula because of Galactic confusion, this would imply a *higher* mass-loss rate, although this correction is expected to be less than a factor of ~ 2 or 3 , assuming the line profile is symmetric.

4.2.2. *Is a Significant Fraction of the Circumstellar Material Swept from the ISM?*

As mass-losing stars move through the ISM, their jetsam can be augmented by material swept from the local ISM. The fraction of the circumstellar envelope that originates in this manner will depend on a combination of the stellar mass, the stellar wind parameters, and the ambient ISM density (Villaver et al. 2002). Accounting for this swept-up interstellar

mass is important in evaluating the true mass-loss rate from the star.

In the absence of a detailed numerical model, we can obtain a crude estimate of the amount of swept-up material in the circumstellar environment of δ Cephei as $M_s = \int_0^{t_{ml}} \pi r^2 V_s \rho dt$, where r is the effective radius of the star, V_s is its space velocity, ρ is the mass density of the ambient medium, and t_{ml} is the length of time that the star has been losing mass.

Adopting an ISM particle density $n \approx 10 \text{ cm}^{-3}$ (see § 4.2.3) translates to $\rho = 1.7 \times 10^{-23} \text{ g cm}^{-3}$. Assuming $r=0.107 \text{ pc}$ (Marengo et al. 2010b), $V_s=10.3 \text{ km s}^{-1}$ (§ 1), and $t_{ml}=90,600 \text{ yr}$ (§ 4.2), this yields $M_s \approx 0.01(n_{\text{HI}}/10 \text{ cm}^{-3})(t_{ml}/90,600 \text{ yr}) M_\odot$, or roughly 14% of the directly observed H I mass. Even after allowing for factors of a few uncertainty in both n and t_{ml} , this supports our interpretation of the emission detected by the VLA as arising predominantly from a wind from δ Cephei. This is also consistent the conclusions of Marengo et al. (2010b), who argued that the low inferred PAH content of the material detected by *Spitzer* implies that it is dominated by debris originating in the stellar wind. In the future, more sophisticated numerical simulations (cf. Villaver et al. 2002) could help to obtain more accurate constraints on M_s .

4.2.3. Comparison with Previously Derived Mass-Loss Rates for δ Cephei

Based on their *Spitzer* measurements, Marengo et al. (2010b) used two independent approaches to estimate a mass-loss rate for δ Cephei in the range $\dot{M} \approx 5 \times 10^{-9}$ to $6 \times 10^{-8} M_\odot \text{ yr}^{-1}$. If we scale these values to account for revised stellar space velocity of $V_s=10.3 \text{ km s}^{-1}$ adopted in the present work (see § 1) and the outflow velocity of $V_o \approx 35.6 \text{ km s}^{-1}$ inferred from the H I data, this translates to $\dot{M} \approx 7.2 \times 10^{-9}$ and $2.1 \times 10^{-8} M_\odot \text{ yr}^{-1}$, respectively. These values are consistent with theoretically predicted mass-loss rates for Cepheids (Neilson & Lester 2008), but are significantly lower than the values that we infer from the H I data.

The smaller of the two mass-loss rate values from Marengo et al. (2010b) was derived based on the observed stand-off distance of the bow shock structure together with ram pressure balance arguments. The implied mass-loss rate could be higher if the local ISM particle density in the vicinity of δ Cephei is larger than the originally adopted value of $n = 0.55 \text{ cm}^{-3}$. Indeed, there is evidence that a higher particle density in the region is plausible. Fernie (1990) derived a reddening value of $E(B - V) = 0.092$ toward δ Cephei; assuming $A_V/E(B - V)=3.1$ (Savage & Mathis 1979), this implies a V -band extinction coefficient $A_V \approx 0.29$. Such a value is typical of interstellar clouds with $n \approx 10\text{-}50 \text{ cm}^{-3}$

(Turner 1997). We note that owing to its larger angular extent, the circumstellar dust detected by *Spitzer* should contribute negligibly to A_V . Assuming a typical grain radius $a=0.001\mu\text{m}$, a total dust mass $M_{\text{dust}}=6\times 10^{-7} M_{\odot}$, and a radial extent $r=0.103$ pc (Marengo et al. 2010b), then $A_{V,\text{local}} \sim 0.22M_{\text{dust}}a^{-1}r^{-2} \approx 0.01$. Finally, from the database of Kalberla et al. (2005), the H I column density along the line-of-sight to δ Cephei is $N_{\text{HI}} = 7.7 \times 10^{21} \text{ cm}^{-2}$, implying a mean particle density out to the distance of the star of $n \approx 9.2 \text{ cm}^{-3}$. This is again consistent with a local particle density several times higher than the canonical Galactic plane value for warm, intercloud H I (cf. Dickey & Lockman 1990). Assuming a local ISM density with $n \sim 10 \text{ cm}^{-3}$ would imply $\dot{M} \sim 1.4 \times 10^{-7} M_{\odot} \text{ yr}^{-1}$ based on ram pressure balance arguments, in somewhat better agreement with our H I-derived value given the uncertainties in both estimates.

The second mass-loss rate estimate from Marengo et al. (2010b) was derived under the assumption that the gas-to-dust (g/d) ratio of the circumstellar material has a value of 100, typical of what is found in the ISM and in the circumstellar environments of AGB stars. However, it is presently unknown whether this value should hold in the circumstellar environment of a Cepheid. For example, the ratio g/d is found to be 5-10 times higher than the canonical value in the circumstellar envelopes of some supergiants (e.g., Skinner & Whitmore 1988), presumably because grain condensation has been incomplete in the winds of such stars (Mauron & Josselin 2011). Even more extreme values may be plausible in the winds of Cepheids owing to their higher temperatures and higher ultraviolet fluxes. In the case of δ Cephei, $g/d \approx 2300$ would be needed to reconcile the mass-loss rate of Marengo et al. (2010b) with our H I estimates. Interestingly, such a value would be self-consistent in the sense that the empirically derived mass volume density of the dusty wind, ρ_{OF} , would then match the density for a wind with $\dot{M} \approx 1 \times 10^{-6} M_{\odot} \text{ yr}^{-1}$ and $V_{\text{o}}=35.6 \text{ km s}^{-1}$ as predicted by the mass continuity equation for stellar winds: $\dot{M} = 4\pi\rho_{\text{OF}}r^2V_{\text{o}}$ (Lamers & Cassinelli 1999).

In summary, our best estimate of the mass-loss rate of δ Cephei based on the combined results from our VLA H I data and *Spitzer* infrared data is $\dot{M} \approx (1 \pm 0.8) \times 10^{-6} M_{\odot} \text{ yr}^{-1}$. The quoted error bar reflects the dominant systematic uncertainties and is based on the dispersion in the values derived from the independent methods presented in the preceding sections.

4.3. Implications of the Empirically Derived Mass-Loss Rate for Theoretical Models of Cepheids

4.3.1. Consistency with Theoretically Predicted Mass Loss Rates

The majority of Cepheids for which mass-loss rates (or upper limits) have previously been determined (§ 1) are inferred to have \dot{M} values at least two or three orders of magnitude smaller than we have derived for δ Cephei in the present work. We emphasize however, that none of these previous determinations exclude the possibility of significant mass-loss through a predominantly neutral atomic wind, of the type we have detected through H I observations. In the case of δ Cephei, the wind also revealed its presence through FIR emission, although this need not be the case for all mass-losing Cepheids, particularly those with higher effective temperatures (where dust grains might be destroyed more readily), those that lack a companion (which may play a role in exciting FIR emission), or those residing in lower density environments (where dust swept from the ISM might contribute negligibly to the circumstellar FIR emission). It is clear that an H I survey of a larger sample of Cepheids will be needed to obtain a better understanding of the importance of these factors and to assess the ubiquity of Cepheid mass loss that is traceable through H I 21-cm line emission.

Based on theoretical studies to date, the most promising physical mechanism by which Cepheids could lose significant mass appears to be the enhancement of radiatively driven mass loss through shocks and pulsation (Willson & Bowen 1984; Neilson & Lester 2008). From analytic models of this type, Neilson & Lester (2008) and Neilson et al. (2011) predicted typical Cepheid mass-loss rates in the range 10^{-10} to $10^{-7} M_{\odot} \text{ yr}^{-1}$, although these rates are highly sensitive to the balance of forces and the adopted physical parameters for a given star. In particular, for shorter periods (smaller masses), the mass-loss rate has a non-linear dependence on the stellar mass. Thus for a Cepheid with the mass and period of δ Cephei, it appears that the models of Neilson & Lester and Neilson et al. can in principle accommodate mass-loss rates as high as $10^{-6} M_{\odot} \text{ yr}^{-1}$, consistent with our VLA findings (H. Neilson, private communication). However, this conclusion may change if mass loss is highly episodic (see below).

4.3.2. The Effects of Mass Loss on the Pulsation Period

Secular period changes are well known to occur in Cepheids, but are generally assumed to be dominated by evolutionary effects (which result in changes in the effective temperature and luminosity) rather than mass loss (Turner et al. 2006). It is therefore of considerable interest to compare the change in pulsation period for δ Cephei, \dot{P} , that is predicted to

occur as a result of its derived mass loss rate with the value of \dot{P} previously derived from observational data.

Equation 62 of Neilson & Lester (2008) provides an analytic formula for estimating the effect of mass loss on the rate of change in the stellar pulsation period. The most extreme period changes due to mass loss are expected to occur when changes in both T_{eff} and L (and hence R) are minimal. Moreover, the time scale for the decrease in total mass is predicted to be faster than the canonical evolutionary time scale. Under these conditions, the period changes dominated by mass-loss should always be positive. If we take the pulsation period and pulsation mass for δ Cephei from Table 1, together with $\dot{M} = 10^{-6} M_{\odot} \text{ yr}^{-1}$, using Equation 62 of Neilson & Lester we estimate the period change as a result of mass loss from δ Cephei to be $\dot{P} = 0.06 \text{ s yr}^{-1}$. This is in apparent contradiction to the observed value of $\dot{P} = -0.1 \text{ s yr}^{-1}$ derived for δ Cephei by Berdnikov et al. (2000) based on data spanning 130 years. This suggests that mass loss is only one contributor to the secular period change and that evolutionary effects on the star following mass loss cannot be ignored. An additional consideration is that mass loss inside the instability strip may be episodic. This could explain, for example, why most previous searches for Cepheid mass loss (which have only been sensitive to material in close proximity of the star) have typically implied much lower rates of mass-loss than we infer from the VLA and *Spitzer* observations of δ Cephei. However, in order to account for the same total amount of matter shed, highly episodic mass loss would require a boost in efficiency of the Cepheid mass loss mechanism.

4.3.3. *Could the Mass Loss Have Occurred During an Earlier Evolutionary Phase?*

One of the few Cepheids that has been previously inferred to have a mass loss rate comparable to the rate we have derived for δ Cephei in our present study is RS Pup, where $\dot{M} \approx 10^{-6} M_{\odot} \text{ yr}^{-1}$ (Deasy 1988; Barmby et al. 2011). RS Pup is unique among Galactic Cepheids in that it is surrounded by a prominent reflection nebula. The linear extent of this nebula ($\sim 1 \text{ pc}$) is comparable to the H I nebula that we measure toward δ Cephei. Although the origin of RS Pup’s nebulosity is consistent with copious mass loss, some authors have argued that the bulk of the nebular material may have originated during an earlier evolutionary phase, either as a Be star (Kervella et al. 2009) or as a red giant (Havlen 1972). The question of whether such arguments could also be applied to δ Cephei is important, since it impacts whether subsequent mass loss during the Cepheid phase will be sufficient to reconcile the Cepheid mass discrepancy for this star.

The geometry of the nebula that we observe surrounding δ Cephei places strong constraints on this issue. The presence of an infrared-emitting bow shock and a head-tail struc-

ture to the H I nebula strongly suggest that δ Cephei has *ongoing* mass-loss. While this alone does not exclude the possibility that some portion of the material in its circumstellar nebula was shed during an earlier evolutionary phase (e.g., at the tip of the red giant branch), the fact that the dynamical age of the H I nebula is smaller than the predicted duration of the second crossing of the instability strip for δ Cephei (see § 4.5) suggests a strong likelihood that the bulk of the mass loss occurred during the Cepheid evolutionary phase. Further, the dynamical age of the nebula implies that even if some of the mass were lost during the red giant phase, this is likely to have immediately preceded the current Cepheid crossing. Hence the resulting mass loss would still necessitate a change in the evolutionary mass of the star between its first and its second (current) Cepheid crossing.

4.4. Comments on the Inferred Outflow Velocity for the δ Cephei Wind and Its Implication for the Mass Loss Mechanism

In § 4.2.1, we estimated an asymptotic (outflow) velocity for the δ Cephei wind of $V_o \approx 35.6 \text{ km s}^{-1}$. To our knowledge, this is the first directly measured outflow velocity for a Cepheid. An important characteristic of this value is that it is significantly smaller than the stellar escape velocity. Adopting the mean stellar radius and pulsation mass for δ Cephei quoted in Table 1, the escape velocity from the photospheric surface of δ Cephei is $V_{\text{esc}} \approx 200 \text{ km s}^{-1}$, or several times the asymptotic velocity. While the radius and effective surface gravity of δ Cephei change over the course of its pulsation cycle, these effects are not sufficient to change this conclusion. Andrievsky et al. (2005) reported changes in the effective surface gravity of δ Cephei by a factor of 5.6, which implies that even when the surface gravity is at its minimum, the escape velocity would still be $V_{\text{esc}} \approx 120 \text{ km s}^{-1}$. δ Cephei thus appears to share one of the defining characteristics of the cool winds of AGB stars and late-type supergiants, where measured outflow velocities are in general several times smaller than the photospheric escape speed (i.e., $V_o \ll V_{\text{esc}}$; see Holzer & MacGregor 1985; Judge & Stencel 1991). Interestingly, δ Cephei also appears to adhere to the empirical relation $V_o \sim 1.6 \times 10^{-3} V_{\text{esc}}^2$ found by Reimers (1977) based on observations of K giants and G and K supergiants (see also Judge 1992), although the significance of this is unclear, since the physical underpinnings of this relation are poorly understood (Reimers 1977) and δ Cephei is not expected to be undergoing mass loss via the same mechanism as the stars in Reimers’ sample.

As discussed by Holzer & MacGregor (1985), the condition that $V_o \ll V_{\text{esc}}$ has important implications for understanding and constraining the mechanism(s) driving a stellar wind. For example, this requires the existence of some type of regulatory processes such that

most of the driving energy of the wind goes into lifting material out of the stellar gravitational field rather than accelerating the flow. It follows that the inferred momentum flux of the wind, $\dot{M}V_\infty$, represents only a small fraction of the overall energy required to drive the wind. An additional implication is that most of the energy added to the wind must be in the form of momentum rather than heat.

4.5. A Possible Solution to the Cepheid Mass Discrepancy for δ Cephei?

A fundamental question raised by our new empirically derived mass-loss rate for δ Cephei is whether this degree of mass loss can reconcile the mass discrepancy for the star. As described above, δ Cephei is believed to be on its second crossing of the instability strip. The total duration of this evolutionary stage (as well as for the first and third crossings) has previously been calculated for Cepheids with different masses and metallicities by Bono et al. (2000a). However, these models did not include the effects of mass loss and therefore their direct application of the case of δ Cephei will not yield self-consistent results. To overcome this problem, we computed new intermediate-mass evolutionary models specifically for δ Cephei. The theoretical framework we employed was developed by Pietrinferni et al. (2004). The evolutionary tracks we adopted are available in the BaSTI data base⁴ and were constructed by assuming a scaled solar chemical mixture and a fixed solar chemical composition with helium and metal abundances of $Y=0.273$ and $Z=0.02$, respectively.

Several lines of empirical evidence support the occurrence either of mild convective core overshooting during the central hydrogen burning phases of intermediate mass stars (Barmina et al. 2002; Cordier et al. 2002; Cassis & Salaris 2011; Evans et al. 2011) or of enhanced post-main sequence mass loss (Bono et al. 2002; Natale et al. 2008; Cantiello et al. 2011). However, to constrain the effects of different mass loss rates, our current canonical evolutionary models were constructed by neglecting extra-mixing sources both at the edge of the convective core and at the bottom of the convective envelope (Alongi et al. 1991). We plan to provide a more detailed discussion of the impact of the mass loss on the evolutionary properties of helium burning intermediate-mass stars in a forthcoming paper (Bono et al., in preparation).

Figure 5 shows H-R diagrams for evolutionary tracks at a fixed initial stellar mass ($M_\star = 5M_\odot$) but different assumptions concerning the mass-loss rate. Each panel shows the evolutionary phases just before and soon after helium burning, i.e. the so-called “blue loop”. The solid lines denote the predicted first overtone blue (hot) edge and the fundamental red

⁴A few selected evolutionary tracks were specifically computed by A. Pietrinferni for this project.

(cool) edge of the Cepheid instability strip according to Bono et al. (2000b). The triangle and the diamond mark the onset (tip of the red giant branch) and the end of central helium burning phases, respectively. The evolutionary time spent inside the instability strip is also indicated. The evolutionary track plotted in the top panel was constructed by neglecting mass loss. The track plotted in the middle panel was constructed by assuming a mass loss starting from the main sequence phase according to the semi-empirical formula from Reimers (1975):

$$\dot{M} = 4 \times 10^{-13} \eta \frac{(L/L_{\odot})(R/R_{\odot})}{M/M_{\odot}} \quad (2)$$

The free parameter η was fixed at 0.4 (Pietrinferni et al. 2004; Bono et al. 2006). Following this prescription, the mass loss rate during the evolution of the star will vary according to the changes in surface luminosity and radius. However, a comparison of the theoretical predictions plotted in the two top panels of Figure 5 shows that the impact of the mass loss based on the prescription of Reimers is negligible, and indeed, both the extent in effective temperature of the blue loop and the evolutionary time spent inside the instability strip are minimally affected. Plausible increases in the free parameter η do not change this outcome, and the Reimers model cannot produce sufficient mass loss to account for the observed quantity of circumstellar material around δ Cephei, nor can it reconcile the mass discrepancy for this star.

Finally, in the bottom panel of Figure 5, we show an evolutionary track with the same initial mass of the top panels, but assuming a steady mass loss rate of $\dot{M} = 5 \times 10^{-7} M_{\odot} \text{ yr}^{-1}$ during the evolutionary phases inside the Cepheid instability strip. As expected, we found that implementing such mass-loss causes a significant decrease in the extent in effective temperature of the blue loop owing to the decrease in the envelope mass (Bono et al. 2000a, and references therein), and in turn a decrease in the evolutionary time spent inside the instability strip. We also explored models with higher mass-loss rates (not shown), but found that for $\dot{M} \gtrsim 10^{-6} M_{\odot} \text{ yr}^{-1}$, the temperature extent of the blue loop becomes significantly smaller, leading to implausibly short Cepheid lifetimes.

To further constrain the impact of the initial stellar mass, we computed an additional set of evolutionary models with an initial stellar mass $M_{\star} = 6M_{\odot}$ (Figure 6). The evolutionary tracks show a behavior similar to the $M_{\star} = 5M_{\odot}$ models when moving from the case of no mass-loss (top) to the Reimers mass-loss case (middle) to the case of mass loss inside the instability strip at a rate of $\dot{M} = 5 \times 10^{-7} M_{\odot} \text{ yr}^{-1}$ (bottom). As with the $M_{\star} = 5M_{\odot}$ models, higher mass-loss rates ($\dot{M} \gtrsim 10^{-6} M_{\odot} \text{ yr}^{-1}$) destroyed the blue loop, resulting in a negligible lifetime on the instability strip.

The above findings indicate that either (1) the true mass-loss rate from δ Cephei is at the low end of our empirically derived range, or (2) that a more complex treatment of mass loss is required (e.g., episodic mass loss or implementation of multi-dimensional Eulerian hydrodynamic and stellar evolution codes; Mocák et al. 2009). The inclusion of extra mixing and stellar rotation may also be important. We consider possibility (1) below, while possibility (2) will be explored in future works.

If we assume that δ Cephei is currently near the midst of its second crossing of the instability strip, the models presented in Figures 5 and 6 predict that a Cepheid with the chemistry and evolutionary mass of δ Cephei and undergoing mass loss at a rate of $\dot{M} = 5 \times 10^{-7} M_{\odot} \text{ yr}^{-1}$ will have so far spent roughly $(0.9\text{--}3.0) \times 10^5$ yr on the instability strip (most of it on the second crossing). These numbers are consistent with the dynamical age of the H I wake estimated in § 4.2.1. Steady mass-loss at the prescribed rate over such an interval is predicted to result in a mass of circumstellar material of ~ 0.04 to $0.15 M_{\odot}$. The upper end of this range is consistent with our empirically derived estimate for the mass of circumstellar material after correction for He (§ 4.2.1), implying that such a model is self-consistent. Moreover, this amount of material is remarkably close to the change in mass required to reconcile the pulsation and evolutionary masses of δ Cephei ($M_e - M_p \approx 0.2 - 1.8 M_{\odot}$ assuming that $M_e = 5.5 \pm 0.5 M_{\odot}$). We conclude that to within current observational and theoretical uncertainties, *mass loss offers a tenable solution to resolving a significant fraction of the the mass discrepancy for δ Cephei.*

From observations of only a single star, we cannot draw any general conclusion about the ubiquity or evolutionary importance of mass loss from Cepheids. Furthermore, as discussed in § 1, a general solution to the mass discrepancy for all Cepheids is likely to require a combination of both mass-loss and overshoot. However, since only the mass loss can be observed directly, future efforts to identify large-scale circumstellar debris around a larger sample of Cepheids and a comparison of these results with theoretical models (including evolutionary models and non-linear convective hydrodynamic models) are likely to provide powerful new constraints on the relative contributions of mass loss versus overshoot for Cepheids of various masses.

5. Conclusions

We have used the VLA to search for H I 21-cm line emission in the circumstellar environment of the archetype of Cepheid variables, δ Cephei. We have detected an extended ($13'$, or ~ 1 pc) nebula at the position of the star. The nebula exhibits a head-tail morphology, with the head of the structure aligning closely with the infrared-emitting nebula and

bow shock previously detected by Marengo et al. (2010b), while the tail appears to be a turbulent structure that trails the motion of the star through the ISM. We measure an H I mass for the nebula of $M_{\text{HI}} \approx 0.07 M_{\odot}$, although its total H I mass could be ~ 2 -3 times larger, depending on the fraction of emission that is hidden by the strong Galactic emission that contaminates a portion of our observing band. Additional material may also be present on large angular scales ($\gtrsim 15'$) to which the VLA is insensitive. We interpret the bulk of the H I nebula surrounding δ Cephei as arising from a stellar wind with a mass-loss rate of $\dot{M} \approx (1.0 \pm 0.8) \times 10^{-6} M_{\odot} \text{ yr}^{-1}$ and an outflow velocity $V_o \approx 35 \text{ km s}^{-1}$. By computing evolutionary models that include mass loss across the instability strip, we show that a mass-loss rate of this magnitude, sustained over the preceding Cepheid lifetime of δ Cephei, could be sufficient to resolve a significant fraction of the longstanding discrepancy between the masses of the star derived from stellar pulsation versus stellar evolutionary models.

It is a pleasure to thank A. Pietrinferni for the computation of several evolutionary tracks and for many insightful discussions concerning the evolutionary properties of intermediate-mass stars. We are also grateful to H. Neilson for valuable discussions concerning Cepheid mass loss. The observations presented here were obtained through NRAO program AM998. LDM acknowledges support for this work from grant AST-1009644 from the National Science Foundation. NRE acknowledges support from the Chandra X-ray Center, NASA contract NAS8-03060.

REFERENCES

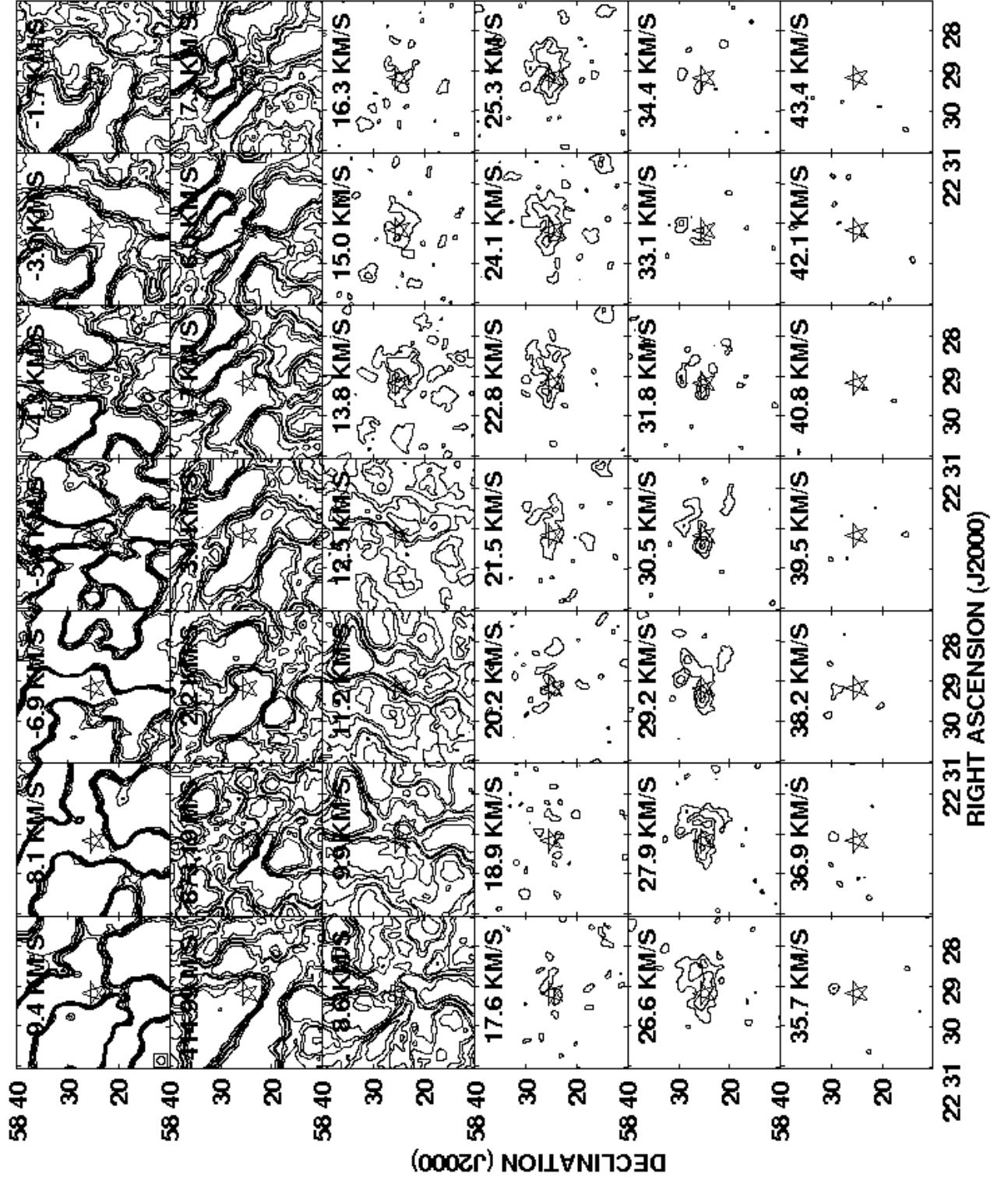
- Alongi, M., Bertelli, G., Bressan, A., & Chiosi, C. 1991, *A&A*, 244, 95
- Andrievsky, S. M., Luck, R. E., & Kovtyukh, V. V. 2005, *ApJ*, 130, 1880
- Armstrong, J. T., Nordgren, T. E., Germain, M. E., Hajian, A. R., Hindsley, R. B., Hummel, C. A., Mozurkewich, D., & Thessin, R. N. 2001, *AJ*, 121, 476
- Barmby, P. Marengo, M., Evans, N. R., Bono, G., Huelsman, D., Su, K. Y. L., Welch, D. L., & Fazio, G. G. 2011, *AJ*, 141, 42
- Barmina, R., Girardi, L., & Chiosi, C. 2002, *A&A*, 385, 847
- Begum, A. et al. 2010, *ApJ*, 722, 395
- Benedict, G. F. et al. 2002, *AJ*, 124, 1695
- Berdnikov, L. N., Ignatova, V. V., Caldwell, J. A. R., & Koen, C. 2000, *New Astron.*, 4, 625
- Bohm-Vitense, E. & Love, S. G. 1994, *ApJ*, 420, 401

- Bono, G., Caputo, F., Cassisi, S., Marconi, M., Piersanti, L., & Tornambè, A. 2000a, *ApJ*, 543, 955
- Bono, G., Caputo, F., & Castellani, V. 2006, *Mem. S. A. It.*, 77, 207
- Bono, G., Castellani, V., & Marconi, M. 2000b, *ApJ*, 529, 293
- Bono, G., Castellani, V., & Marconi, M. 2002, *ApJ*, 565, L83
- Bowers, P. F. & Knapp, G. R. 1988, *ApJ*, 332, 299
- Cantiello, M., Braithwaite, J., Brandenburg, A., Del Sordo, F., Käpylä, P., & Langer, N. 2011, *IAU Symposium* 272, 32
- Caputo, F., Bono, G., Fiorentino, G., Marconi, M., & Musella, I. 2005, *ApJ*, 629, 1021
- Cenarro, A. J. et al. 2007, *MNRAS*, 374, 664
- Ciosi, C., Wood, P. R., Bertelli, G., Bressan, A., & Mateo, M. 1992, *ApJ*, 385, 205
- Comerón, F. & Kaper, L. 1998, *A&A*, 338, 273
- Condon, J. J., Cotton, W. D., Greisen, E. W., Yin, Q. F., Perley, R. A., Taylor, G. B., & Broderick, J. J. 1998, *AJ*, 115, 1693
- Cordier, D., Lebreton, Y., Goupil, M.-J., Lejeune, T., Beaulieu, J.-P., & Arenou, F. 2002, *A&A*, 392, 169
- Cox, A. N. 1980, *ARA&A*, 18, 15
- Deasy, H. P. 1988, *MNRAS*, 231, 673
- Deasy, H. & Butler, C. J. 1986, *Nature*, 320, 726
- Deutsch, A. 1960, in *Aerodynamic Phenomena in Stellar Atmospheres*, *IAU Symposium No. 12 on Cosmical Gas Dynamics*, ed. R. N. Thomas, 238
- Dickey, J. M. & Lockman, F. J. 1990, *ARA&A*, 1990, 28, 215
- Evans, N. R. 2009, in *Stellar Pulsation: Challenges for Theory and Observations*, ed. J. A. Guzik and P. A. Bradley (American Institute of Physics), 69
- Evans, N. R., Berdnikov, L., Gorynya, N., Rastorguev, A., & Eaton, J. 2011, *AJ*, 142, 87
- Feast, M. W. & Walker, A. R. 1987, *ARA&A*, 25, 345
- Fernie, J. D. 1990, *ApJS*, 72, 153
- Freedman, W. L. et al. 2001, *ApJ*, 553, 47
- Gautschy, A. & Saio, H. 1996, *AR&A*, 34, 551
- Gérard, E. & Le Bertre, T. 2006, *AJ*, 132, 2566
- Greisen, E. W. & Liszt, H. S. 1986, *ApJ*, 303, 702

- Havlen, R. J. 1972, *A&A*, 16, 252
- Heiles, C. & Troland, T. H. 2003, 586, 1067
- Holzer, T. E. & MacGregor, K. B. 1985, in *Mass Loss from Red Giants*, ed. M. Morris and B. Zuckerman, (Dordrecht: Reidel), 229
- Iben, I. Jr. 1974, *ARA&A*, 12, 215
- Iglesias, C. A., Rogers, F. J., & Wilson, B. G. 1990, *ApJ*, 360, 221
- Isaacman, R. 1979, *A&A*, 77, 327
- Jorissen, A. et al. 2011, *A&A*, 532, A135
- Judge, P. G. 1992, in *Seventh Cambridge Workshop on Cool Stars, Stellar Systems, and the Sun*, ASP Conf. Series, 26, ed. M. S. Giampapa & J. A. Bookbinder (San Francisco: ASP), 403
- Judge, P. G. & Stencel, R. E. 1991, *ApJ*, 371, 357
- Kalberla, P. M. W., Burton, W. B., Hartmann, D., Arnal, E. M., Bajaja, E., Morras, R., & Pöppel, W. G. L. (2005), *A&A*, 440, 775
- Keller, S. C. & Wood, P. R. 2006, *ApJ*, 642, 834
- Kervella, P., Mérand, A., & Gallenne, A. 2009, *A&A*, 498, 425
- Kervella, P., Mérand, A., Perrin, G., & Coudé du Foresto, V. 2006, *A&A*, 448, 623
- Knapp, G. R. & Bowers, P. F. 1983, *ApJ*, 266, 701
- Ladjal, D. et al. 2010, *A&A*, 518, L141
- Lamers, H. J. G. L. M. & Cassinelli, J. P. 1999, *Introduction to Stellar Winds*, (Cambridge: Cambridge University Press)
- Libert, Y., Le Bertre, T., Gérard, E., & Winters, J. M. 2008, *A&A*, 491, 789
- Marengo, M., Evans, N. R., Barmby, P., Bono, G., Welch, D. L., & Romaniello, M. 2010a, *ApJ*, 709, 120
- Marengo, M., Evans, N. R., Barmby, P., Matthews, L. D., Bono, G., Welch, D. L., Romaniello, M., Huelsman, D., Su, K. Y. L., & Fazio, G. G. 2010b, *ApJ*, 725, 2392
- Martin, D. C. et al. 2007, *Nature*, 448, 780
- Matthews, L. D. & Reid, M. J. 2007, *AJ*, 133, 2291
- Matthews, L. D., Libert, Y., Gérard, E., Le Bertre, T., & Reid, M. J. 2008, *ApJ*, 684, 603
- Matthews, L. D., Libert, Y., Gérard, E., Le Bertre, T., Johnson, M. C., & Dame, T. M. 2011, *AJ*, 141, 60

- Mauron, N. & Josselin, E. 2011, *A&A*, 526, 156
- Mérand, A., Aufdenberg, J. P., Kervella, P., Coudé du Foresto, V., ten Brummelaar, T. A., McAlister, H. A., Sturmann, L., Sturmann, J., & Turner, N. H. 2007, *ApJ*, 664, 1093
- Mocák, M., Müller, E., Weiss, A., & Kifonidis, K. 2009, *A&A*, 501, 659
- Natale, G., Marconi, M., & Bono, G. 2008, *ApJ*, 674, 93
- Neilson, H. R., Cantiello, M., & Langer, N. 2011, *A&A*, 529, L9
- Neilson, H. R. & Lester, J. B. 2008, *ApJ*, 684, 569
- Neilson, H. R., Ngeow, C.-C., Kanbur, S. M., & Lester, J. B. 2009, *ApJ*, 692, 81
- Noriega-Crespo, A., Van Buren, D., Cao, Y., & Dgani, R. 1997, *AJ*, 114, 837
- Olofsson, H., Eriksson, K., Gustafsson, B., & Carlstrom, U. 1993, *ApJS*, 87, 267
- Perley, R. A. & Taylor, G. B. 2003, *VLA Calibration Manual* (<http://www.vla.nrao.edu/astro/calib/manual/index.shtml>)
- Pietrinferni, A., Cassisi, S., Salaris, M., & Castelli, F. 2004, *ApJ*, 612, 168
- Raga, A. C., Cantó, J., De Colle, F., Esquivel, A., Kajdic, P., Rodríguez-González, A., & Velázquez, P. F. 2008, *ApJ*, 680, L45
- Reimers, D. 1975, *Mem. Soc. Roy. Sci. Liège*, 8, 369
- Reimers, D. 1977, *A&A*, 57, 395
- Roberts, M. S. 1975, in *Galaxies and the Universe*, ed. A. Sandage et al. (Chicago: University of Chicago Press), 309
- Sahai, R. & Chronopoulos, C. K. 2010, *ApJ*, 711, L53
- Samus, N. N. et al. 2011, *General Catalog of Variable Stars*, Version 2011Jan (<http://www.sai.msu.su/gcvs>)
- Savage, B. D. & Mathis, J. S. 1979, *ARA&A*, 17, 73
- Schönrich, R., Binney, J., & Dehnen, W. 2010, *MNRAS*, 403, 1829
- Seaton, M. J., Yan, Y., Mihalas, D., & Pradhan, A. K. 1994, *MNRAS*, 266, 805
- Skinner, C. J. & Whitmore, B. 1988, *MNRAS*, 235, 603
- Turner, B. E. 1997, in *Astrophysical Implications of the Laboratory Study of Presolar Materials*, ed. T. J. Bernatowicz and E. K. Zinner (American Institute of Physics), 477
- Turner, D. G., Abdel-Sabour Abdel-Latif, M., & Berdnikov, L. N. 2006, *PASP*, 118, 410
- Ueta, T. et al. 2006, *ApJ*, 648, L39
- Ueta, T. 2008, *ApJ*, 687, L33

- Ueta, T. et al. 2008, PASJ, 60, 407
- Ueta, T. et al. 2010, A&A, 514, 16
- Van Buren, D. & McCray, R. 1988, ApJ, 329, L93
- Verschuur, G. L 1974, ApJS, 27, 65
- Villaver, E., García-Segura, G., & Manchado, A. 2002, ApJ, 571, 880
- Wareing, C. J., Zijlstra, A. A., & O’Brien, T. J. 2007a, ApJ, 660, L129
- Wareing, C. J., Zijlstra, A. A., O’Brien, T. J., Seibert, M. 2007b, ApJ 670, L125
- Wareing, C. J., et al. 2006, MNRAS, 372, L63
- Welch, D. L. & Duric, N. 1988, AJ, 95, 1794
- Wilkin, F. P. 1996, ApJ, 459, L31
- Willson, L. A. & Bowen, G. H. 1984, Nature, 312, 429
- Wilson, R. E. 1953, General Catalogue of Stellar Radial Velocities, Carnegie Institute of Washington Publication 601



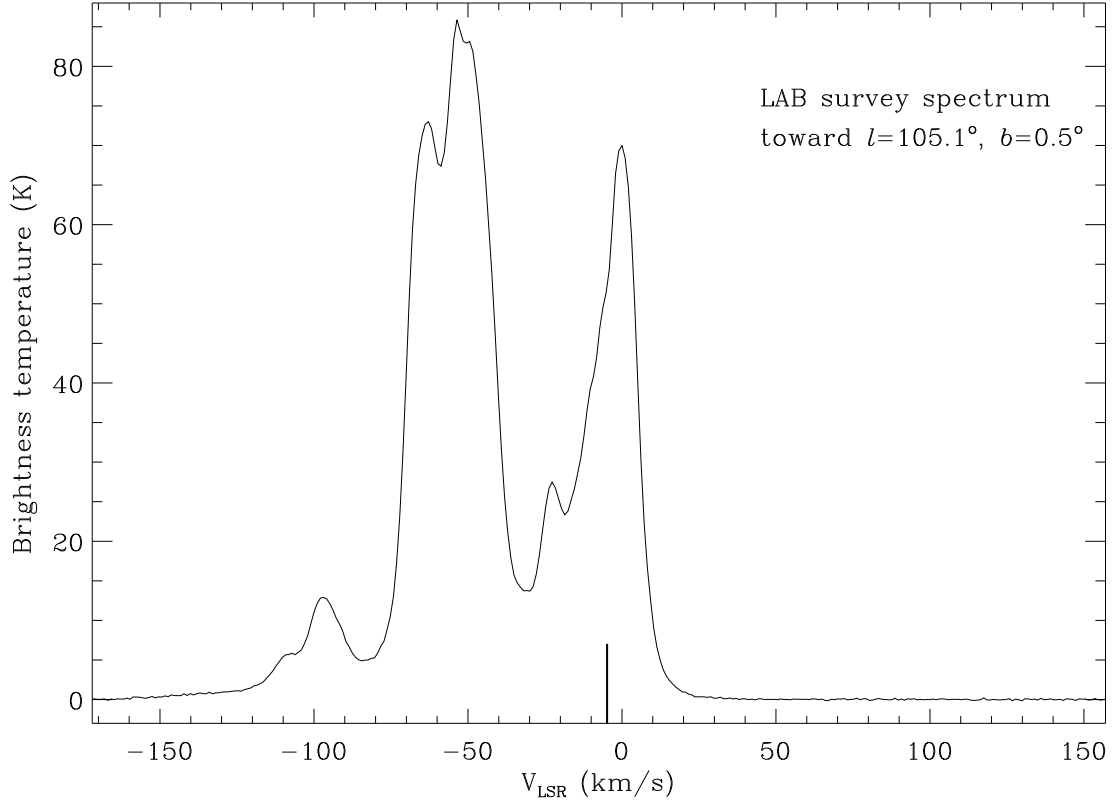


Fig. 2.— Single-dish H I spectrum toward $l = 105^\circ.1$, $b = 0^\circ.5$, illustrating the nature of the Galactic emission along the line-of-sight to δ Cephei. The data were taken from Kalberla et al. 2005. The velocity range shown corresponds to our VLA observing band. The vertical bar indicates the systemic velocity of δ Cephei. Note that the rms noise level in this spectrum (~ 0.09 K or ≈ 0.57 Jy) is too high to permit detection of circumstellar emission even in the uncontaminated portion of the band.

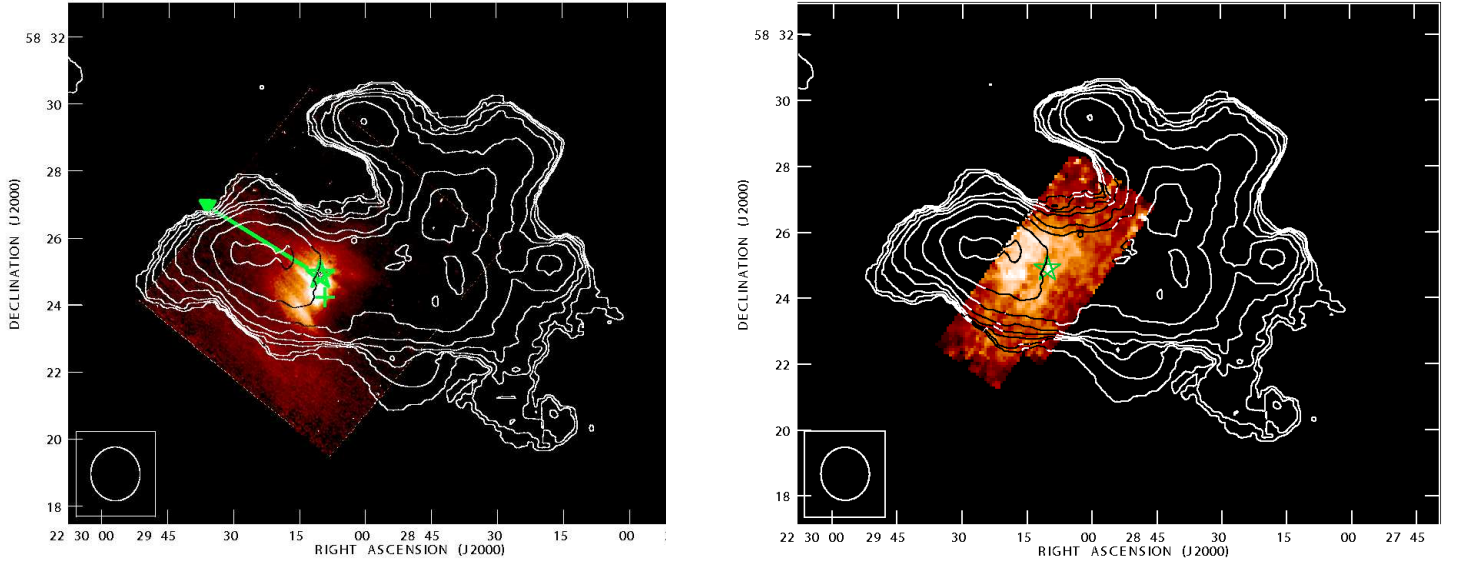


Fig. 3.— H I total intensity contours overlaid on *Spitzer* 24 μ m (left) and 70 μ m (right) images from Marengo et al. 2010b. The H I contour levels are $(1, 1.4, 2, \dots, 11.3) \times 18 \text{ Jy beam}^{-1} \text{ m s}^{-1}$. The positions of δ Cephei and its companion HD 213307 are indicated by star and plus symbols, respectively. The direction of space motion of δ Cephei with respect to the ISM is indicated by a green arrow on the left panel. The insets in the lower left corners of each panel indicate the size of the VLA synthesized beam ($96'' \times 88''$).

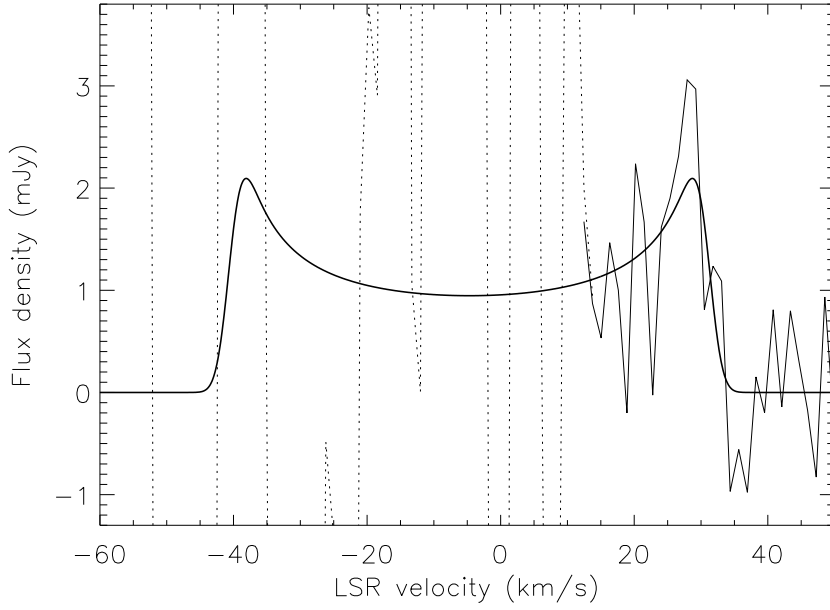


Fig. 4.— Observed VLA H I spectrum toward the position of δ Cephei, averaged over a single synthesized beam centered on the star (thin lines), with the best-fitting model H I spectrum overplotted as a thick line (see § 4.2.1 for details). The observed spectrum was extracted from the “Robust+1” data cube (see Table 3). The portion of the observed spectrum indicated by a dotted line is heavily contaminated by Galactic emission and was excluded from the fit.

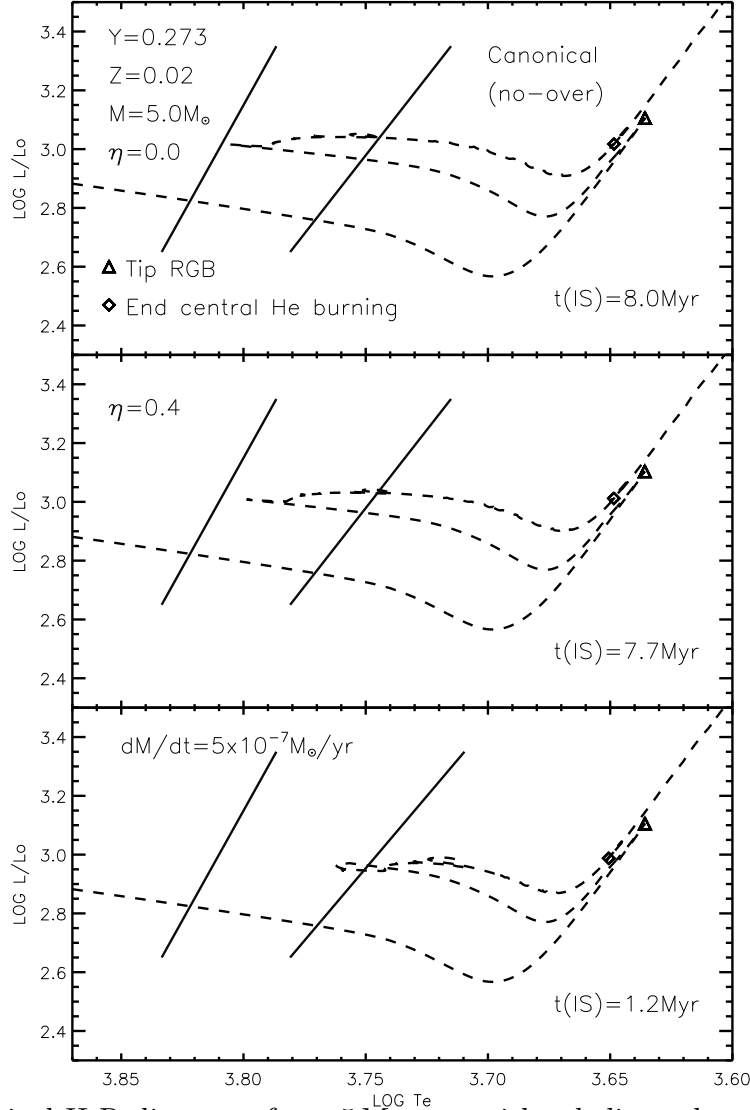


Fig. 5.— Theoretical H-R diagrams for a $5M_{\odot}$ star with a helium abundance $Y=0.273$ and metal abundance $Z=0.02$. The dashed lines indicate the evolutionary path of the star. The solid lines depict the boundaries of the instability strip. The top panel shows a canonical model with no mass loss. The center panel includes mass loss starting on the main sequence and following a Reimers law with $\eta=0.4$ (Eq. 2). The lower panel shows a model where mass loss with a rate $\dot{M}=5 \times 10^{-7} M_{\odot} \text{ yr}^{-1}$ turns on at the red edge of the instability strip and continues throughout the Cepheid phase. The total time spent on the instability strip for each of the models is indicated in the lower right corner. No overshoot is included. See § 4.5 for further details.

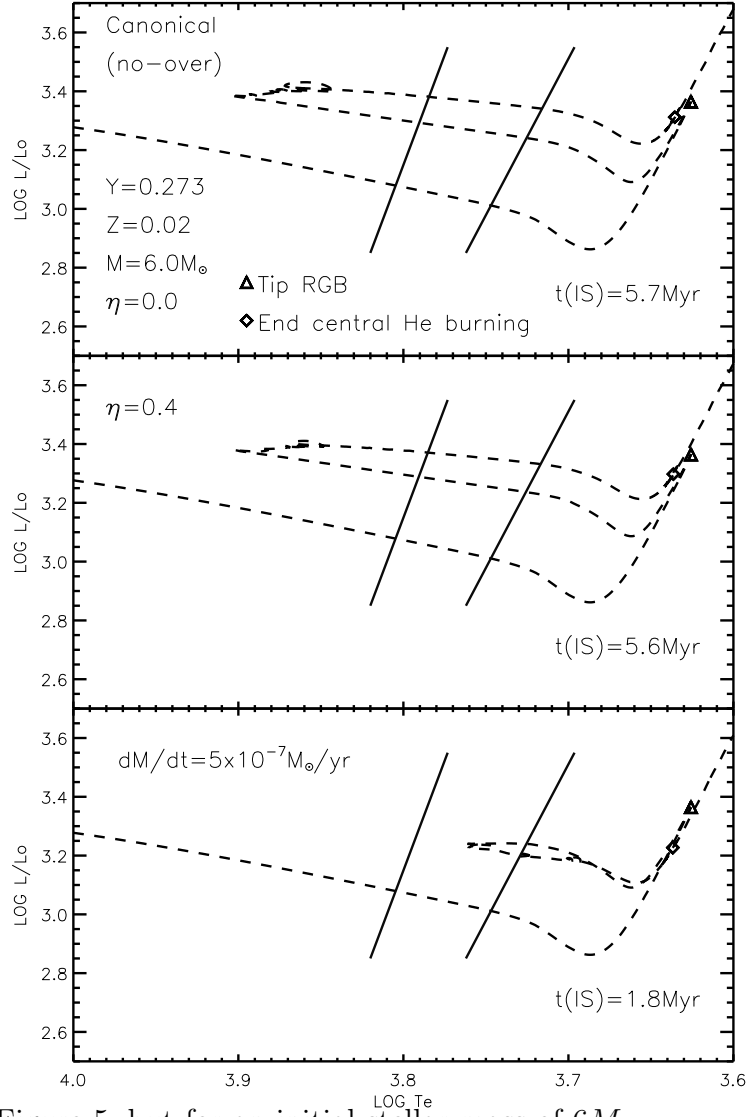


Fig. 6.— As for Figure 5, but for an initial stellar mass of $6M_{\odot}$.